Excess pore pressure generation in silty sands subjected to cyclic triaxial loading

Xiao Wei i), Yansheng Zhuang ii), Jun Yang iii), Lisha Zhang iv)

- i) Associate Researcher, Zhejiang University, Hangzhou, China.
- ii) Research Assistant, University of Hong Kong, Hong Kong, China iii) Professor, University of Hong Kong, Hong Kong, China
- iv) Associate Professor, Hangzhou City College, Hangzhou, China

ABSTRACT

Liquefaction of sands is a result of excess pore water pressure generation due to the contractive tendency of the soil skeleton under undrained cyclic shearing. Proper characterization of the excess pore water pressure plays an important role in liquefaction analyses. In this paper, we present results from a series of cyclic triaxial tests on silty sands with different fines contents. Based on these results, we put forward two pore water pressure models (a stress-based model and an energy-based model) to characterize the pore pressure built-up, where the model parameters are calibrated regarding different fines contents, packing densities, confining pressures, and loading amplitudes. The methods for characterizing the model parameters are also discussed.

Keywords: liquefaction, silty sand, pore pressure generation, stress-based model, energy-based model

1 INTRODUCTION

Soil liquefaction due to earthquakes remains an unsolved problem, and it still causes catastrophic consequences in recent major earthquakes (Mason et al. 2019; Yasuda et al. 2012). Positive generation of excess pore pressure in a soil element subjected to cyclic loading reduces the effective stress, and thus, compromises the resistance of soils against all kinds of external loading. For this reason, it is crucial to characterize the excess pore pressure adequately for liquefaction analyses.

Many pore pressure models have been proposed in the past and can be broadly categorized into three major types, namely, stress-based models (Booker et al. 1976), strain-based models (Vucetic and Dobry 1986), and energy-based models (Davis and Berrill 1982). For the stress-based models and the strain-based models, irregular seismic loadings are converted into uniform stress or strain cycles with certain assumptions. For the energy-based models, it relates the residual excess pore pressure to the energy dissipated by the soil element. It should be noted that most of these investigations focused on the liquefaction of medium-dense to dense soils that failed in the pattern of cyclic mobility (Castro 1969).

Most of the early investigations used clean sands for laboratory testing, however, liquefied natural sands usually contain certain amounts of fines. This study conducts stress-controlled cyclic triaxial tests on silty sands and investigates the excess pore pressure generation characteristics. A stress-based model and an

energy-based model are used to characterize the excess pore pressure generations of silty sands.

2 MATERIALS AND TESTING PROGRAM

Toyoura sand mixed with non-plastic silica silt was used for laboratory testing. Fig. 1 presents the particle size distributions of the clean Toyoura sand, silica silt, and two tested sand-silt mixtures with fines contents (FC) of 10% and 20%. TSS10 and TSS20 are designations of the two mixtures with FC = 10% and 20%, respectively.

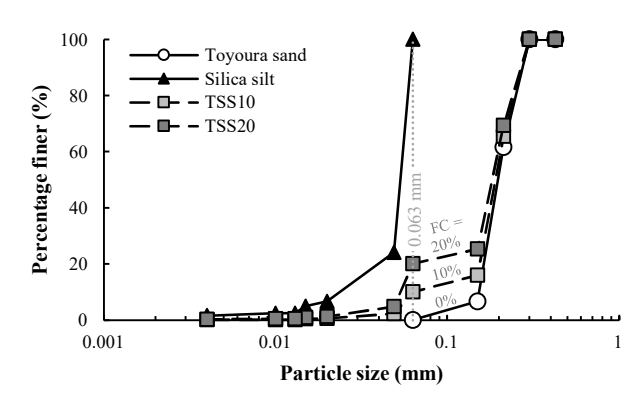


Fig. 1 Particle size distribution of the tested materials

All specimens were reconstituted by moist tamping method and saturated following the same procedures used by (Wei and Yang 2023). The dry sand was mixed thoroughly with water at a water content of 5%, and then, compacted in a split mold to form a specimen with a

diameter of 71.1 mm and a height of 142.2 mm in six layers. Specimens were saturated by conducting percolation of CO₂, circulation of de-aired water, and application of back pressures in sequence. A specimen with a B-value higher than 0.98 is considered to be fully saturated. The saturated specimens were isotropically consolidated before the cyclic shearing. Sinusoidal deviatoric stress cycles were used for cyclic loading, and the amplitude is represented by the cyclic stress ratio (CSR), which is defined as follows,

$$CSR = \frac{q_{cyc}}{2\sigma'_{rc}} \tag{1}$$

where $q_{\rm cyc}$ is the amplitude of the deviatoric stress cycles; $\sigma'_{\rm nc}$ is the effective normal stress on the maximum shear stress plane of the specimens under triaxial stress condition, which is equal to the mean effective stress (p') after consolidation for the isotropic stress state. Using $\sigma'_{\rm nc}$ instead of $\sigma'_{\rm 3c}$ is a common practice for analysis of cyclic triaxial test data (e.g., Ishihara 1996). Table 1 summarizes the testing plan. In this paper, representative experimental data are selected for conciseness.

Table 1. Testing plan

Materials	Target void ratio (e)	Effective stress (σ'_{nc})
0.791	40, 100, 300 kPa	
0.847	100 kPa	
0.903	100, 300 kPa	
0.910	100 kPa	
TSS20	0.717	100 kPa
	0.791	40, 100, 300 kPa
	0.847	100 kPa
	0.903	100 kPa
	0.920	100 kPa

3 FAILURE PATTERNS

Fig. 2 presents typical results of a specimen that failed in the pattern of cyclic mobility. Typical features include the large development of axial strain (ε_a) when the deviatoric stress (q) returned to zero (Fig. 2(a)), butterfly-type stress path (Fig. 2(b)), and transient liquefied states that the excess pore pressure (Δu) reaches the value of the initial effective stress (Fig. 2(c)). Fig. 3 presents typical test results of a specimen that fails in the pattern of unlimited flow. This type of failure is characterized by rapid development of axial strain without significant pre-failure strain accumulation (Fig. 3(a)). In the case shown in Fig. 3, the specimen liquefied after the flow failure took place. However, the flow deformation is so rapid that the triaxial apparatus cannot record any test data during the flow, and dashed lines are used in Fig. 3 to schematically represent the behavior during the flow. In Fig. 2(c) and Fig. 3(c), the grey dots represent the residual excess pore water pressure ($\Delta u_{\rm res}$). These points are obtained at the end of each cycle, where the deviatoric stress returns to zero.

Different failure criteria are applied to different failure patterns. The attainment of 5% double amplitude of axial strain is defined as the failure for cyclic mobility, and the onset of flow is defined as the failure for flow-type failure. Then, the number of cycles to cause failure (N_f) can be determined for specimens with different initial states (in terms of void ratio and effective confining pressure) that were loaded by different amplitudes.

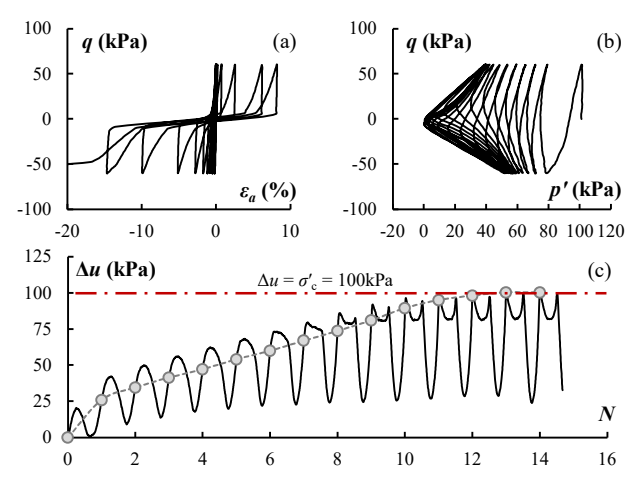


Fig. 2 Cyclic mobility, TSS20, $e_c = 0.721$, $\sigma'_{nc} = 100$ kPa

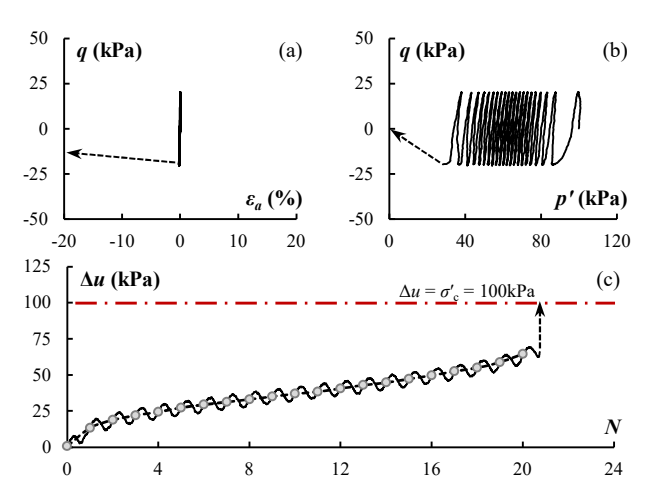


Fig. 3 Flow-type failure, TSS20, $e_c = 0.905$, $\sigma'_{nc} = 100$ kPa

4 EXCESS PORE PRESSURE MODELS

The pore water pressure ratio, $R_{\rm u}$, is calculated according to the following equation,

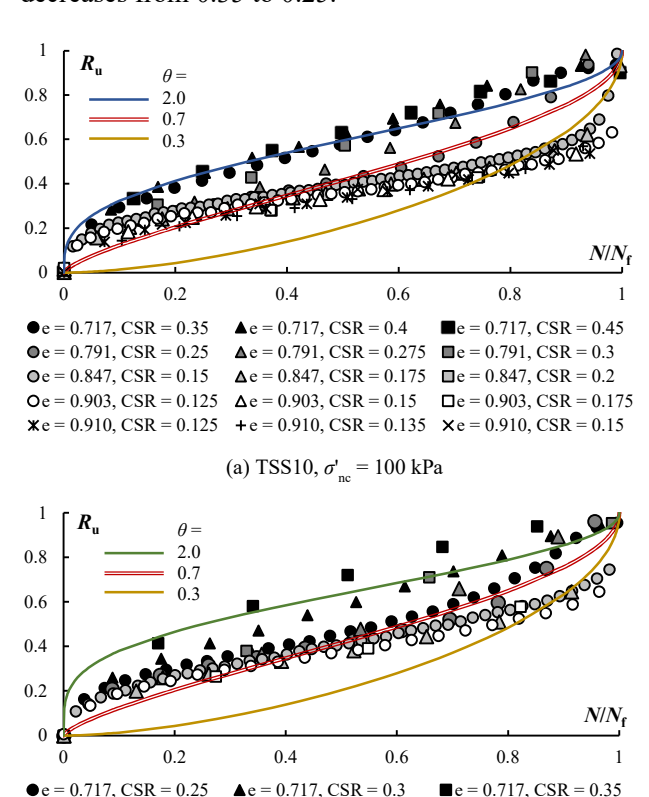
$$R_u = \frac{\Delta u}{\sigma'_{\text{max}}} \tag{2}$$

which is a commonly used dimensionless pore pressure index.

4.1 Stress-based model

For a specimen that fails under several uniform stress cycles, it is straightforward to define N and $N_{\rm f}$. Thus, the $R_{\rm u}$ - $N/N_{\rm f}$ relationship obtained at the end of each cycle

conveniently represents the pore pressure generation for stress-based approaches. Fig. 4 presents the R_u - N/N_f relationships of TSS10 and TSS20 under $\sigma'_{nc} = 100 \text{ kPa}$, showing a general trend that the R_u - N/N_f relationships shift downwards with increasing void ratios. Taking TSS10 (Fig. 4(a)) as an example, the data of specimens with e = 0.717 form the upper bound, and the data of specimens with e = 0.903 and 0.910 form the lower bound, leaving the data of specimens with e = 0.791 and 0.847 in between. In addition, the data of specimens with e = 0.847 are located lower than those of e = 0.791 and are very close to the lower bound. However, scrutiny of the test data indicates that CSR can also influence the $R_{\rm u}$ - $N/N_{\rm f}$ relationships in some cases. For example, the $R_{\rm u}$ - $N/N_{\rm f}$ data from TSS10 specimens with e = 0.791 in Fig. 4(a) moves downwards when CSR decreases from 0.3 to 0.25, and the R_u - N/N_f data from TSS20 specimens with e = 0.717 in Fig. 4(b) moves downwards when CSR decreases from 0.35 to 0.25.



(b) TSS20, $\sigma'_{nc} = 100$ kPa Fig. 4 R_u -N/N_f relationships of two silty sands under $\sigma'_{nc} = 100$ kPa

 $\Phi e = 0.791 \text{ CSR} = 0.2$

 $\Theta e = 0.847$, CSR = 0.125

 \Box e = 0.903, CSR = 0.125

Booker et al. (1976) proposed the following model to characterize the R_u - N/N_f relationships,

$$R_u = \frac{2}{\pi} \sin^{-1} \left(\frac{N}{N_f} \right)^{\frac{1}{2\theta}} \tag{3}$$

 $\Delta e = 0.791$, CSR = 0.225 $\Box e = 0.791$, CSR = 0.25

 $\Delta e = 0.847$, CSR = 0.165 Oe = 0.903, CSR = 0.1

where θ is a model parameter. In each plot of Fig. 4, three

curves with different values of θ were compared with the experimental data. It is clear that the model cannot capture the shape of $R_{\rm u}$ - $N/N_{\rm f}$ relationships.

A modified version of the R_u - N/N_f model is given as follows,

$$R_u = 1 - \frac{2}{\pi} \sin^{-1} \left(1 - \frac{N}{N_f} \right)^{\alpha} \tag{4}$$

where α is a model parameter. It gives improved results to simulate the R_u - N/N_f relationships, as shown by Fig. 5 using representative experimental data of TSS10 under $\sigma'_{nc} = 100$ kPa. The curves of the calibrated Eq. 4 agree fairly well with the experimental data of specimens with different packing densities and different failure patterns.

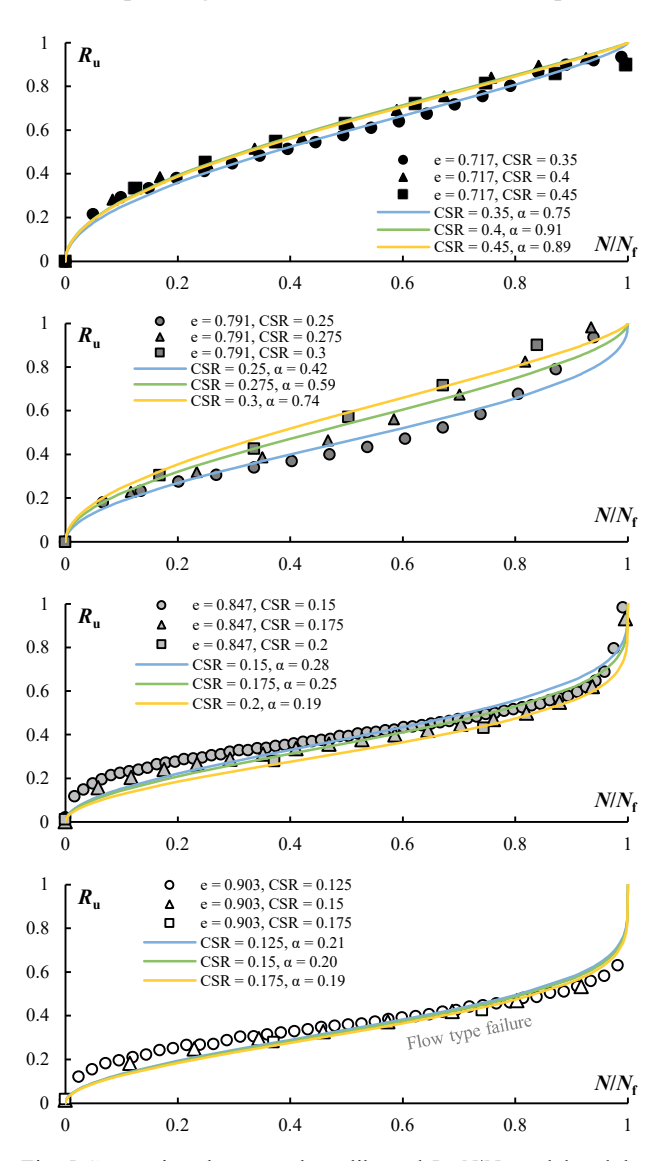


Fig. 5 Comparison between the calibrated $R_{\rm u}$ - $N/N_{\rm f}$ model and the experimental data of TSS10 under $\sigma_{\rm nc}$ = 100 kPa

4.2 Energy-based model

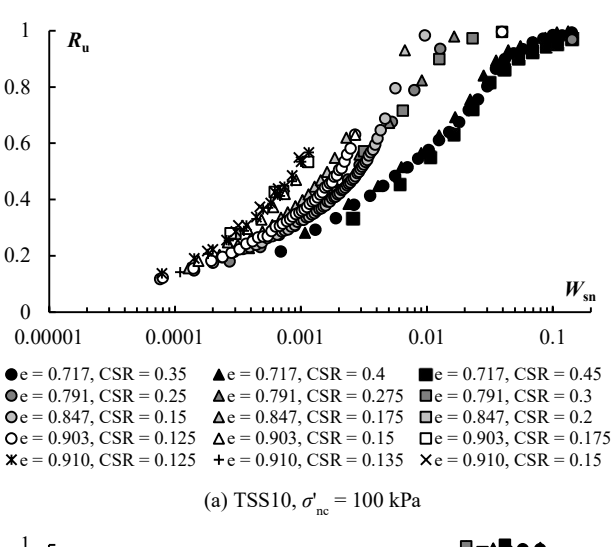
The accumulated strain energy (W_s) can be calculated using the following equation for undrained triaxial tests,

$$W_{s} = \frac{1}{2} \sum (q_{i} + q_{i+1}) \cdot (\varepsilon_{a,i+1} - \varepsilon_{a,i})$$
 (5)

where subscripts i and i + 1 represent two adjacent data points documented by the apparatus. The strain energy can be further normalized by the initial effective stress to become dimensionless, and the stress-normalized accumulative strain energy $(W_{\rm sn})$ is defined as follows,

$$W_{sn} = \frac{W_s}{\sigma'_{nc}} \tag{6}$$

Fig. 6 presents experimental data of the correlation between $R_{\rm u}$ and $W_{\rm sn}$ measured at the end of each cycle. There is a general trend that the $R_{\rm u}$ - $W_{\rm sn}$ relationships shift to the right with a decrease in void ratio, indicating that a higher amount of energy needs to be dissipated for the denser specimens than for the looser specimens to generate the same amount of residual excess pore water pressure.



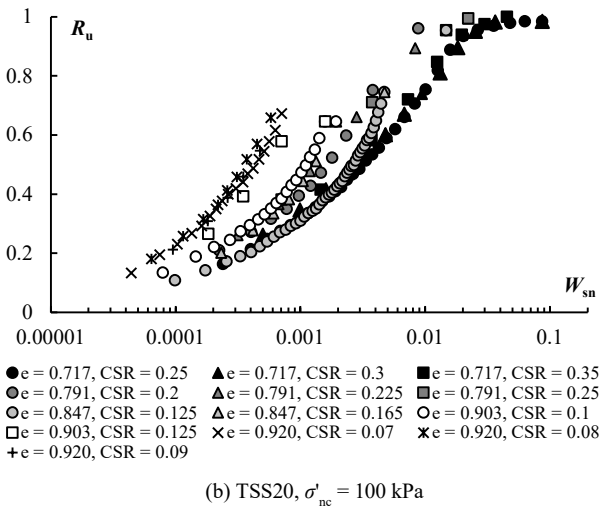


Fig. 6 R_u - W_{sn} relationships of two silty sands under $\sigma'_{nc} = 100$ kPa

Researchers have proposed a variety of energy-based pore pressure models using different types of functions, including power functions, hyperbolic functions, exponential functions, etc (Berrill and Davis 1985; Davis and Berrill 2001; Polito et al. 2008; Porcino et al. 2022). Davis and Berrill (2001) suggested a one-parameter pore pressure model as follows,

$$R_{\rm u} = 1 - \exp\left(-A \cdot W_{\rm sn}\right) \tag{7}$$

where A is a model parameter. Fig. 7 compares the experimental data with the curves of the calibrated models showing good agreement between the model predictions and the experimental data.

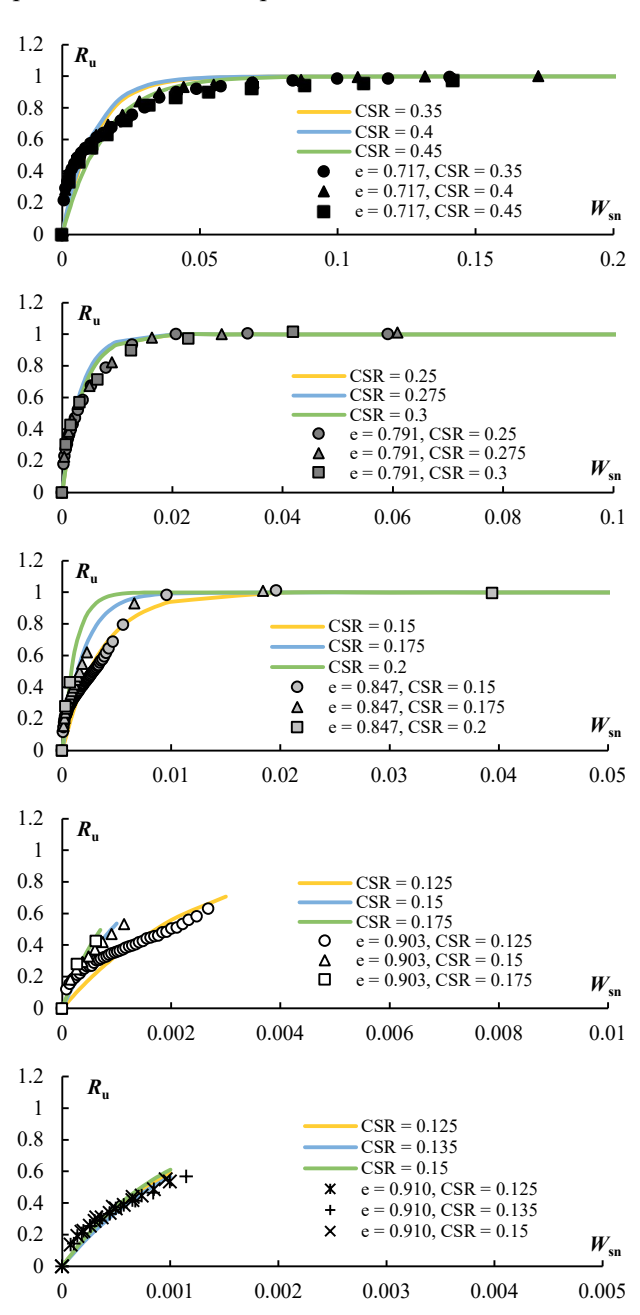


Fig. 7 Comparison between the calibrated R_u - W_{sn} model and the experimental data of TSS10 under σ'_{nc} = 100 kPa

5 MODEL PARAMETERS

The calibrated model parameters of the proposed $R_{\rm u}$ - $N/N_{\rm f}$ model (i.e., α in Eq. 4) are plotted against the void

ratio in Fig. 8(a). There is a general trend that α decreases with increasing void ratio. However, its value may vary significantly for specimens with similar void ratios, depending on factors such as effective confining pressure and CSR. When the calibrated values are plotted against CSR for the TSS10 specimens, it is surprising that a more or less unified relationship can be obtained for specimens with different void ratios and effective confining pressures. A similar trend can also be obtained for TSS20, and the α -CSR relationships for TSS10 and TSS20 are more or less the same (Fig. 8(c)). According to the results shown in Figs. 8(b) and (c), the values of parameter α can be assumed to be constant for the two silty sands when CSR is smaller than 0.2. For cases where CSR is larger than about 0.35, constant α can be proposed for TSS10 while more experimental results are needed for TSS20.

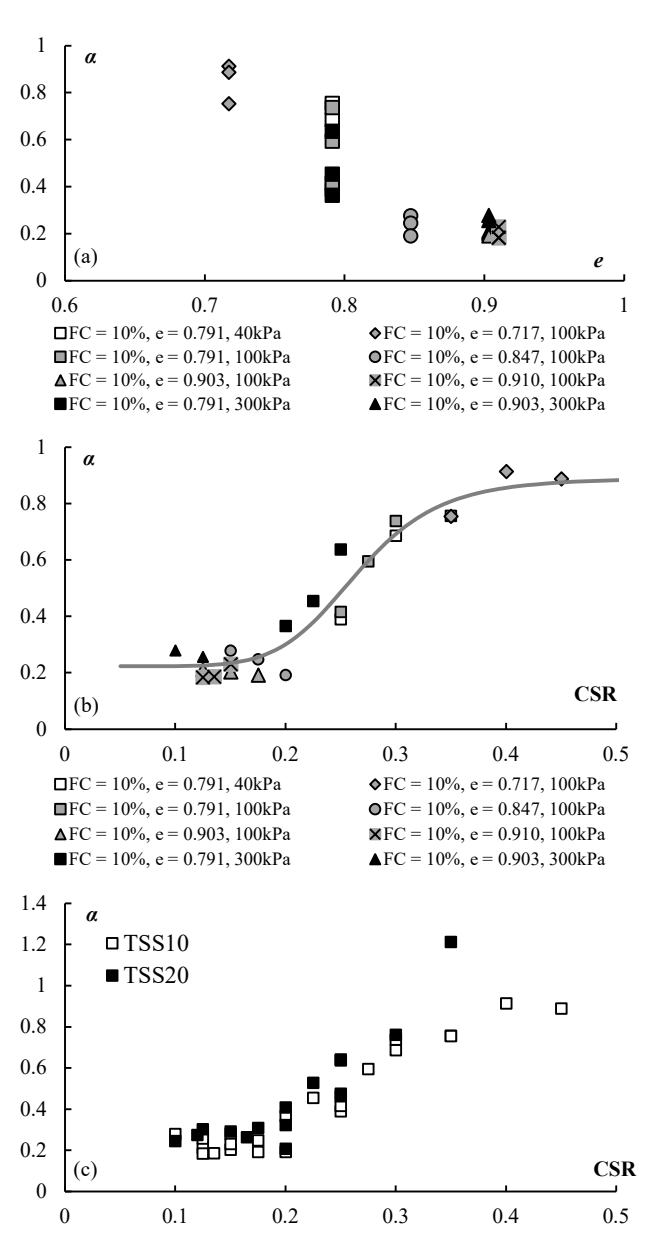
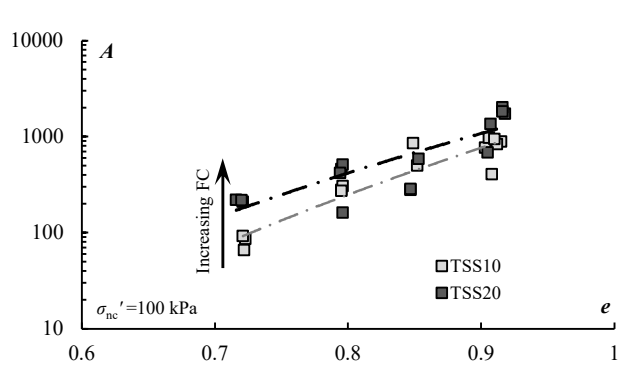
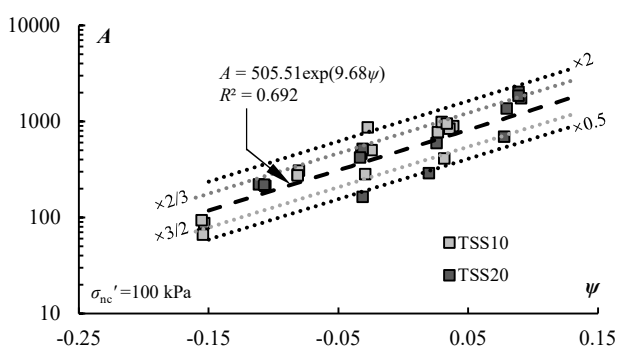


Fig. 8 Calibrated model parameter of the proposed R_u - N/N_f model (Eq. 4)

The one-parameter exponential energy model (Eq. 7) is calibrated using the experimental data of TSS10 and TSS20. The calibrated model parameter A increases with increasing void ratio for a given material under a given effective stress, and it also increases with increasing fines content under otherwise similar conditions (Fig. 9(a)). The results shown in Fig. 9(a) indicate that the Ae relationships are FC-specific. It has been reported by some previous investigations (Wei and Yang 2019, 2023; Yang and Liu 2016) that the state parameter, ψ , (Been and Jefferies 1985) can be used to unify FC-specific correlations of non-plastic silty sands. By plotting A against the state parameter (Fig. 9(b)), a unique trend is obtained. The huge scattering shown in Fig. 9(b) comes from several groups of duplicated specimens that were loaded by different CSRs. The reason causing such scattering is worthy of further investigation.



(a) Parameter A plotted against void ratio



(b) Parameter A plotted against state parameter

Fig. 9 Calibrated model parameter of the one-parameter exponential $R_{\rm u}$ - $W_{\rm sn}$ model (Eq. 7) for TSS10 and TSS20 under $\sigma'_{\rm nc}=100$ kPa

Relative density was not adopted for analyzing the experimental data for several reasons. Firstly, previous investigations on the cyclic liquefaction resistance of silty sands have reported inconsistent findings regarding the effects of FC if the liquefaction resistance is compared at the same relative density, as noted by Wei and Yang (2023). The cause of the inconsistent findings could be the uncertainties when measuring the maximum and minimum void ratios for calculating the relative density, especially for sands containing a certain amount of fines.

Secondly, previous investigations comparing the liquefaction resistance of the silty sands based on void ratio usually have similar conclusions on the effects of fines, namely the liquefaction resistance decreases with increasing FC if the FC is smaller than a transition fines content. Wei et al. (2020) indicated that the particle size disparity ratio between the coarse particles and the fines controls the amount of reduction of liquefaction resistance due to the addition of fines at a given void ratio. Moreover, the void ratio can be easily cast into the framework of critical state soil mechanics. Wei and Yang (2023) have found that the liquefaction resistance of silty sands decreases uniquely with an increase in the state parameter, regardless of void ratio, effective stress, fines content, and types of base sand. Since the liquefaction resistance of sand is closely related to the pore pressure generation, the same state variable, namely the void ratio, was mainly used for the analysis in this investigation.

6 CONCLUSIONS

The characteristics of pore water pressure generation of two silty sands are investigated in the frameworks of stress-based and energy-based approaches. The major conclusions are summarized as follows.

- (1) In the stress-based framework, the R_u - N/N_f relationships are found to be dependent on packing density and cyclic stress ratio in a complicated way.
- (2) A new stress-based pore pressure model is proposed and the model parameter has been calibrated using the experimental data. The model parameter can be uniquely correlated with cyclic stress ratio, regardless of void ratio, effective stress, and fines content (for FC = 10% and 20%).
- (3) In the energy-based framework, the R_u - W_{sn} relationships are primarily dependent on the void ratio of the specimens, while the impact of CSR is not obvious.
- (4) A one-parameter energy-based pore pressure model is calibrated using the experimental data. The model parameter can be uniquely correlated with the state parameter.

ACKNOWLEDGEMENTS

The financial support from the National Natural Science Foundation of China (No. 52108351) and the Research Grants Council of Hong Kong (17250316) is greatly acknowledged.

REFERENCES

1) Been, K. and Jefferies, M. G. (1985): A state parameter for

- sands, Géotechnique, 35 (2), 99-112.
- Berrill, J. B. and Davis, R. O. (1985): Energy dissipation and seismic liquefaction of sands: revised model, *Soils and Foundations*, 25 (2), 106–118.
- Booker, J. R., Rahman, M. S. and Seed, H. B. (1976): A Computer Program for the Analysis of Pore Pressure Generation and Dissipation During Cyclic or Earthquake Loading, *Report No. EERC76-24*, Berkley, US.
- Castro, G. (1969): Liquefaction of sands. *PhD Thesis*, Harvard University.
- Davis, R. O. and Berrill, J. B. (1982): Energy dissipation and seismic liquefaction in sands, *Earthquake Engineering and Structural Dynamics*, 10 (1), 59–68.
- Davis, R. O. and Berrill, J. B. (2001): Pore pressure and dissipated energy in earthquakes—field verification, *Journal* of Geotechnical and Geoenvironmental Engineering, 127 (3), 269–274.
- Ishihara, K. (1996): Soil Behaviour in Earthquake Geotechnics. NewYork, United States: Oxford University Press
- Mason, H. B., Gallant, A. P. Hutabarat, D., Montgomery, J., Reed, A. N., Wartman, J., Irsyam, M., Prakoso, W., Djarwadi, D., Harnanto, D., Alatas, I., Rahardjo, P., Simatupang, P., Kawanda, A., Hanifa, R., (2019): Geotechnical Reconnaissance: The 28 September 2018 M7.5 Palu-Donggala, Indonesia Earthquake, Report No. GEER-061, Geotechnical Extreme Events Reconnaissance Association.
- Polito, C. P., Green, R. A. and Lee, J. (2008): Pore pressure generation models for sands and silty soils subjected to cyclic loading, *Journal of Geotechnical and Geoenvironmental* Engineering, 134 (10), 1490–1500.
- 10) Porcino, D. D., Tomasello, G. and Farzalizadeh, R. (2022): Pore-pressure generation of sands subjected to cyclic simple shear loading: an energy approach. In *Proceedings of the 4th International Conference on Performance Based Design in Earthquake Geotechnical Engineering (PBD-IV 2022)*, Bejing, China, 1674–1682.
- 11) Vucetic, M., and Dobry R. (1986): Pore pressure buildup and liquefaction at level sandy sites during earthquakes. *Report No. CE-86-3*, Troy, New York, USA.
- 12) Wei, X. and Yang, J. (2019): Cyclic behavior and liquefaction resistance of silty sands with presence of initial static shear stress, *Soil Dynamics and Earthquake Engineering*, 122, 274– 289.
- 13) Wei, X. and Yang, J. (2023): Characterising the effect of particle size disparity on liquefaction resistance of non-plastic silty sands from a critical state perspective, *Géotechnique*, 73 (4), 323–336.
- 14) Wei, X., Yang, J., Zhou, Y.-G., and Chen, Y. (2020): Influence of particle-size disparity on cyclic liquefaction resistance of silty sands." *Géotechnique Letters*, 10 (2), 155–161.
- 15) Yang, J. and Liu, X. (2016): Shear wave velocity and stiffness of sand: the role of non-plastic fines. *Géotechnique*, 66 (6), 500–514.
- 16) Yasuda, S., Harada, K., Ishikawa, K. and Kanemaru, Y. (2012): Characteristics of liquefaction in Tokyo Bay area by the 2011 Great East Japan Earthquake, *Soils and Foundations*, 52 (5), 793–810.